Response to reviewer comments
Title: Nascent Titanium/Silicon-Containing Particle Formation in Corona Discharge Assisted Combustion
Journal: Aerosol Research
Ref: ar-2025-41

Reviewer #3: Referee's comments:
This manuscript presents measurements of the (mobility) size distribution functions (SDFs), performed via dilution sampling followed by high-resolution differential mobility analysis (HRDMA), of charged nanoparticles and ions formed in Bunsen-type premixed flames of near-stoichiometric methane/air mixtures and trace amounts of either titanium isopropoxide (TTIP) or tethraethyl orthosilicate (TEOS). The measurements are performed at a fixed but unspecified height above the burner (HAB) of about 9mm (according to the inset of Fig.1), with and without the perturbation of an AC corona discharge generated by two coaxial tungsten needles facing each other radially at HAB =3mm, and two discharge powers (i.e., 56 W and 125 W), both at about 21kHz. The measurements are processed upon performing estimates of the fraction of nanopraticles getting charged in the flame via diffusion and field charging. The objective is to investigate the effects of the plasma discharge on the mechanisms of nanoparticle formation in flames, with some indications of the corona enhancing nucleation but suppressing coagulation. The manuscript includes a good survey of the relevant literature, and the results are interesting and worthy of presentation in the archival literature. On the other hand, I think that the writing style and organization quality of the manuscript need some significant improvements before publication, and I would also ask the authors to address my more specific comments below.
Response: We thank the reviewer for the positive comments. We have addressed the comments and concerns raised by the reviewer to the best of our abilities and look forward to positive feedback on our revision.

Comment 1: *Some details of the experimental method are missing. What is the diameter of the sampling orifice and sampling under pressure? What type and size of (coated or uncoated) thermocouple was used to measure the temperature?*
Response: The diameter of the sampling orifice is 0.1 mm at the bottom of the ¼ inch stainless steel tube HiaT probe. In this study we have used an uncoated type S thermocouple (Pt – 10% Rh) with a spherical bead of bead diameter 0.7 mm. The following descriptions have been added to the methods section of this manuscript:

"For flame temperature measurement, we used a type S thermocouple (Pt – 10% Rh) with an exposed uncoated spherical bead of diameter 0.7 mm. In Fig. 1b, we can see the temperature profile which takes into account the radiative heat losses on the thermocouple bead surface."

"The HiaT dilution sampling probe is a 1/4 inch straight stainless steel with a 0.1 mm diameter orifice."

Comment 2: *The manuscript mentions the height of the (I assume conically shaped) flame being about 6.35mm, and an unquantified elongation of the flame caused by the corona discharge. Can you acquire digital images of the flames with and without the corona discharge during sampling (and possibly also without the dilution probe)?*
Response: We have updated Fig. 1 to include digital images of the flame with and without corona discharge. The images were captured when the dilution probe was not operational.

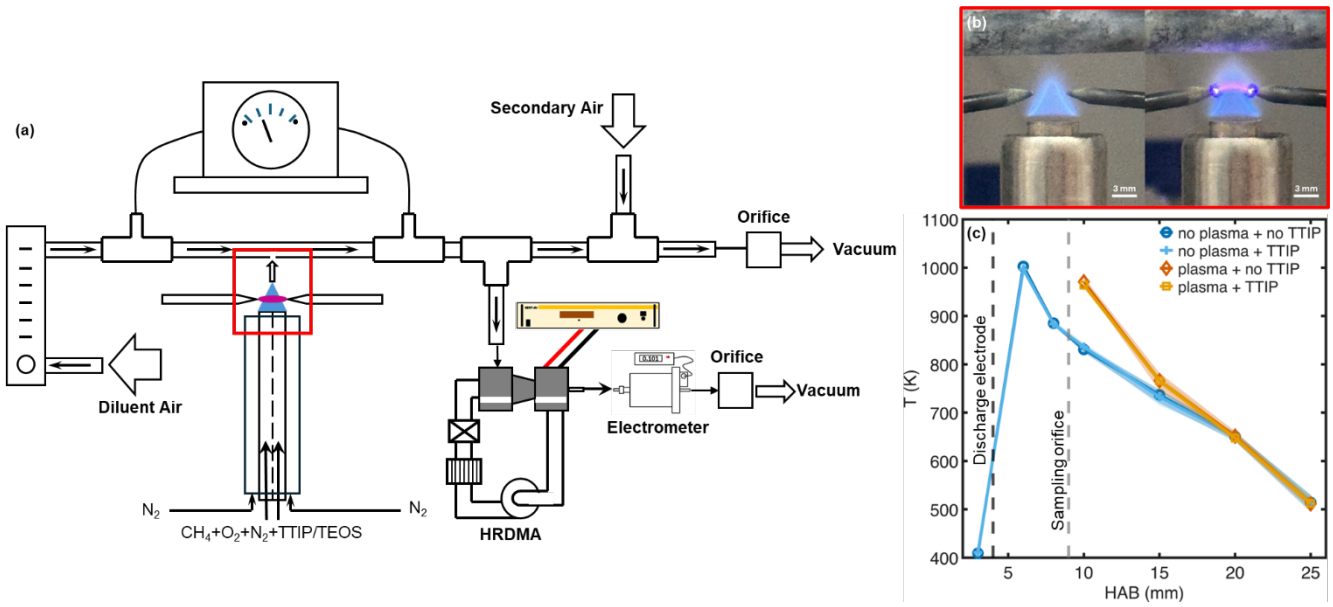

Figure 1: (a) Schematic of the experimental apparatus with a red box highlighting the flame and corona discharge region. (b) Image of flame with and without a corona discharge in the highlighted region. (c) Temperature profile of flames under different plasma and synthesis precursor conditions. The feed rate of TTIP is 19 mg h^{-1} for temperature profile measure, and the plasma power is 125 W.

Comment 3: *The evaluation of the values of the parameter in equations 4 and 5 is not properly described. This is particularly the case for N0 and E0. Also, it is not clear which one of the two equations (or what type of their combination) is used to correct the number concentration of the measured charged particles to report the SDFs.*

Response: We have added more description to the variables associated with Eqs. (4) and (5). Values of all variables including N_0 and E_0 and how they were obtained is now included in the methods section. We have updated the appendix section to reflect the changes. The following is the updated description of the methods section:

"$n_{\text{diff}} = (akT/\epsilon^2)\ \ln(1 + \pi\epsilon^2 caN_0 t/kT)$ (4)

$n_{\text{fld}} = n_s \pi N_0 \epsilon Z t/(\pi N_0 \epsilon Z t + 1)$ (5)

In Eq. (4), a is the particle radius, c is the thermal speed of ions, N_0 is the concentration of ions far away from the particle, ϵ is the elementary unit charge, k is the Boltzmann's constant, t is the exposure time of the particle to unipolar ions, n_{diff} is the charge acquired by the particle due to diffusion charging, n_{fld} is the charge acquired by the particle due to field charging, and T is the temperature in K. We calculate the charge estimates at twenty different logarithmically spaced particle radii, a, ranging from 0.1 to 10 nm. The thermal speed of ions, c, were calculated using Eq. (6) that stem from Maxwell-Boltzmann distribution law. In Eq. (6), m is the mass of ion estimated using the mobility of ions measured from HRDMA and based on the mass-mobility relationship presented by Kilpatrick (Mäkelä et al., 1996). N_0 is the concentration of ions measured in different flame and plasma conditions without precursors as shown in Fig. 2. The value of T is taken as 1003K, the peak temperature measured.

$c = \sqrt[2]{8kT/\pi m}$ (6)

In Eq. (5), Z is the mobility diameter, n_s is the saturation charge. Although not directly used in Eq. (5), the value of the particle's dielectric constant (K) is required to calculate n_s. The saturation charge is calculated using Eq. (7), where E_0 is the intensity of applied electric field. E_0 is calculated from Eqs. (8) and (9), where V_{peak} is the

peak voltage of the AC power source used for both plasma conditions, 56W and 125 W, used in this study and d is the distance between the discharge electrodes. V_{peak} for our experiments is 1.9 KV and d for all experimental conditions is fixed at 3.87 mm.

$$n_s = \{1 + 2[(K-1)/(K+2)]\}(E_0 a^2/\epsilon) \quad (7)$$

$$V_{\text{rms}} = V_{\text{peak}}/\sqrt{2} \quad (8)$$

$$E_0 = V_{\text{rms}}/d \quad (9)$$"

Eqs. (4) and (5) are only used to calculate the charge acquired by the particles due to diffusion and field charging. The method of data inversion is used to correct the number concentration of the measured charged particles. The set of equations used in data inversion are described in our previous work. We have updated the description in our methods section to clarify this. The following is the updated description of the methods section:

"To correct number concentration of the measured charged particles, we performed data inversion as described in our previous work (Bagya Ramesh and Wang, 2024). The data inversion, which accounts for diffusional and penetration losses, increased the number concentration of our measured size distributions to the order of 10^{10} cm^{-3}."

References:

Bagya Ramesh, C. and Wang, Y.: Ions Generated from a Premixed Methane-Air Flame: Mobility Size Distributions and Charging Characteristics, Combustion Science and Technology, 196, 4041–4056, https://doi.org/10.1080/00102202.2023.2203818, 2024.

Mäkelä, J. M., Jokinen, V., Mattila, T., Ukkonen, A., and Keskinen, J.: Mobility distribution of acetone cluster ions, J. Aerosol Sci., 27, 175–190, https://doi.org/10.1016/0021-8502(95)00560-9, 1996.

Comment 4: *The evaluation of the exposure time of particles to the ions based on the flame height is not correct and should, instead, be based on the distance from the blue layer of the flame and the sampling position. This is the case because nanoparticles cannot be formed in the cold, unreacted region upstream of the main reaction zone (i.e., the blue layer) of a premixed flame, unless their formation is caused by the plasma rather than by the flame.*

Response: We thank the reviewer for pointing this out. We redid the exposure time calculations based on the reviewer's correction. The distances between the flame front and the sampling probe were measured from the images shown in Fig. 1b. This distance was 3.27 mm for the flame only condition and 2 mm for the flame with plasma condition. Based on post flame front to sampling probe distance, the exposure time of the particles in flame only condition was calculated to be 3.39 ms and 2.08 ms for flame with a corona discharge of 125W. We have updated the methods section to reflect this change in how we define exposure time. The following is the updated description:

"To estimate the exposure time of particles to ions, we calculated the gas flow velocity and the time that particles remain between post flame region before entering the sampling probe inlet. The volumetric flow rate of the flame was calculated from CH_4, O_2, and N_2 feed rates to be 1.578×10^{-5} m^3 s^{-1}. Dividing the volumetric flow rate with the cross-sectional area of tube burner gave us a flow velocity of 0.962 m s^{-1}. The particles were assumed to be exposed to the ions only for the duration that they spent between the post flame region and the sampling

probe's inlet. By measuring optically using the images shown in Fig. 1b, the flame height was found to be 4.38 mm. In flame only condition, this distance was 3.26 mm, giving an exposure time of 3.9 ms. For the flame with plasma condition, this distance was 2 mm, giving an exposure time of 2.08 ms. These calculations assume that only neutral particles are charged through field charging."

Comment 5: *Related to point D above, it is more than possible that the observed suppression of coagulation is caused by the reduction in the residence time of the particle in the hot post-flame region (where they form) between the flame blue layer and the sampling position, as a result of the flame elongation ensuing the corona discharge.*

Response: We thank the reviewer for pointing this out. We agree that the suppression of coagulation can also be caused due to the reduced residence time. We have added the following description in the results section of the manuscript to convey this possibility to the reader. The added description is as follows:

"However, it is also possible that the suppression in particle growth by coagulation is due to the reduced residence time of the particle in the post flame zone."

Comment 6: *What is the transport time of the aerosol from the sampling orifice to the HRDMA? As reported in the literature you cite, diffusion charging is still active in the diluted flow.*

Response: From inlet of the sampling probe to the inlet of HRDMA, the sampling line is 1.28 m long and based on the aerosol flow rates, the calculated transport time of aerosol is 92.6 ms. We thank the reviewer for pointing this out about diffusion charging. In addition to the exposure time, we have updated our diffusion charging calculations to account for the aerosol transport time in the sampling line. We have added the following description in the methods section of our manuscript to reflect this change:

"The transport time of aerosols from sampling probe inlet to HRDMA inlet is 86.3 ms. During transport, diffusion charging remains active in the diluted flow. Field charging, however, is considered only while the particles are between post flame region and probe inlet, corresponding to the exposure time. Whereas diffusion charging is considered for the entire period between the post flame region and HRDMA inlet, corresponding to the combined exposure time and transport time in sampling line."

Comment 7: *Have all the SDFs in Figs 2-4 been corrected for the estimated charged fraction? How? If not, which ones have been?*

Response: All the size distribution functions shown in Figs. 2, 3, 4, and 5 (Figs. 3 and 4 in the current version of the manuscript.) have been corrected for their number concentration and estimated charged fraction using the data inversion method described in our previous work (Bagya Ramesh and Wang, 2024). The inversion was performed using the equation,

$$\frac{dN}{d\ln D_p} = \frac{\alpha N(V)}{(Q_a/Q_s)\eta_{DET}(D_p)\eta_{pen}(D_p)f_c(D_p)\beta(1+\delta)}$$

The concentration of charged particles (N) is determined by the current (I) measured by electrometer and the dilution ratio, where $N = DR \times I/eQ_{aer}$. Here Q_{aer} is the flow rate through the electrometer in liters per min

and e is the elementary unit of charge. Q_a and Q_s are the inlet and outlet flow rates in the classification zone of HRDMA. α is calculated using D_p and DMA mobilities measured at 298 K. β and δ are dimensionless flow parameters, which are defined by the sheath flow and sampling line flow (Stolzenburg and McMurry, 2008). $\eta_{pen}(D_p)$ is the penetration efficiency of HRDMA, $\eta_{DET}(D_p)$ is the detection efficiency of electrometer, and $f_c(D_p)$ is the charging efficiency. All particles are assumed to be singly charged so $f_c(D_p)$ is taken as 100%. Electrometer is assumed to have $\eta_{DET}(D_p)$ as the issue of potential diffusional losses is addressed through $\eta_{pen}(D_p)$. Cai et al., (2018) presented an empirical formula for calculating penetrating efficiency, $\eta_{pen}(D_p)$, as a function of D_p where $a = 0.82$, $b = 2.57$, $c = 1.56$.

$$\eta_{pen} = a \times \exp\left(-\frac{b}{{D_p}^2}\right) \times \left(-\frac{c}{D_p \times Q_a}\right)$$

The above set of equations and the procedure to correct for the estimated charge fraction is described in detail in our previous work. The description has been updated to clarify this:

"To correct number concentration of the measured charged particles, we performed data inversion as described in our previous work (Bagya Ramesh and Wang, 2024). The data inversion, which accounts for diffusional and penetration losses, increased the number concentration of our measured size distributions to the order of 10^{10} cm^{-3}."

References:

Bagya Ramesh, C. and Wang, Y.: Ions Generated from a Premixed Methane-Air Flame: Mobility Size Distributions and Charging Characteristics, Combustion Science and Technology, 196, 4041–4056, https://doi.org/10.1080/00102202.2023.2203818, 2024.

Cai, R., Attoui, M., Jiang, J., Korhonen, F., Hao, J., Petäjä, T., and Kangasluoma, J.: Characterization of a high-resolution supercritical differential mobility analyzer at reduced flow rates, Aerosol Science and Technology, 52, 1332–1343, https://doi.org/10.1080/02786826.2018.1520964, 2018.

Stolzenburg, M. R. and McMurry, P. H.: Equations governing single and tandem DMA configurations and a new lognormal approximation to the transfer function, Aerosol Science and Technology, 42, 421–432, https://doi.org/10.1080/02786820802157823, 2008.

Comment 8: *It's too easy to lose track of the important message while reading many confusing percentage changes reported in Paragraphs 3.1 and 3.2. This could be substantially improved by changing the current organization of the figures, which highlight the effect of the precursor concentration rather than that of the corona discharge power. Grouping datasets at different powers of the corona discharge in the same panels of the figures (a panel for each precursor type and flow rate) would greatly improve the presentation of the effect of the corona discharge.*

Response: We thank the reviewer for this suggestion. We agree that reorganizing the figures will be very helpful for the user to digest the information presented. We have reorganized Figs. 2, 3, 4, and 5. The updated figures are grouped together based on their precursor feed rate and particle polarity. The three operating conditions, flame, flame with a corona discharge of power 56 W, and flame with a corona discharge of 125 W are all grouped together for every precursor feed rate. The updated figures are given below:

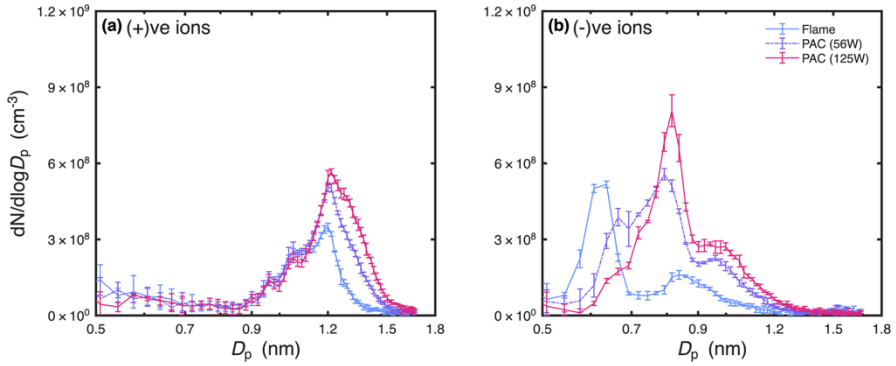

Figure 2: (a) The size distribution of positive ions under flame with and without a corona discharge; (b) The size distribution of negative ions under flame with and without a corona discharge; Both panels show the effect of corona discharge at power 56W and 125W on the ionic size distribution. Error bars denote the standard deviation.

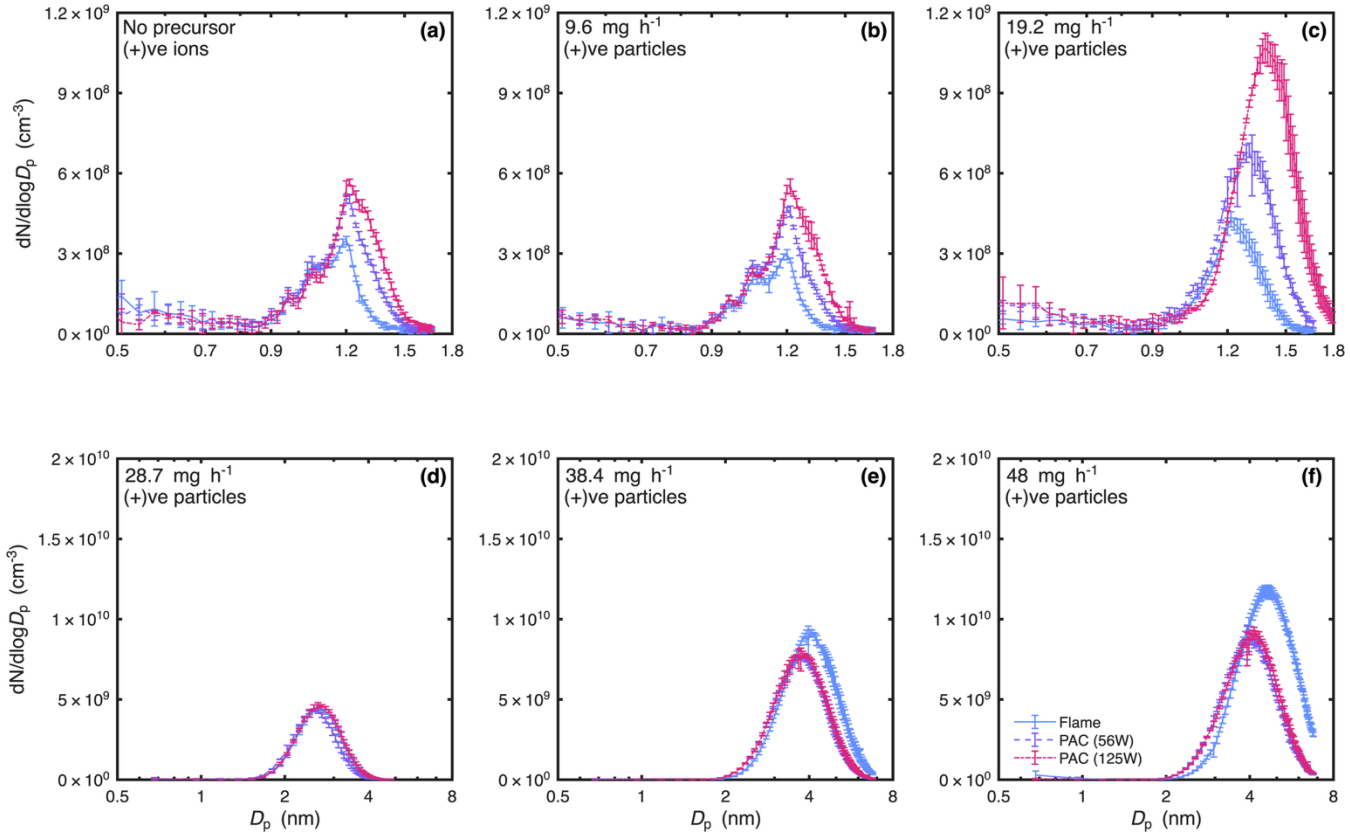

Figure 3: (a) The size distribution of positive ions without any TTIP; (b), (c), (d), (e), and (f) are the size distribution of positively charged Ti-containing clusters with TTIP feed rates ranging from of 9.6 mg h^{-1} to 48 mg h^{-1}. Each panel compares the influence of corona discharge at power 56W and 125W on the size distribution. Error bars denote the standard deviation.

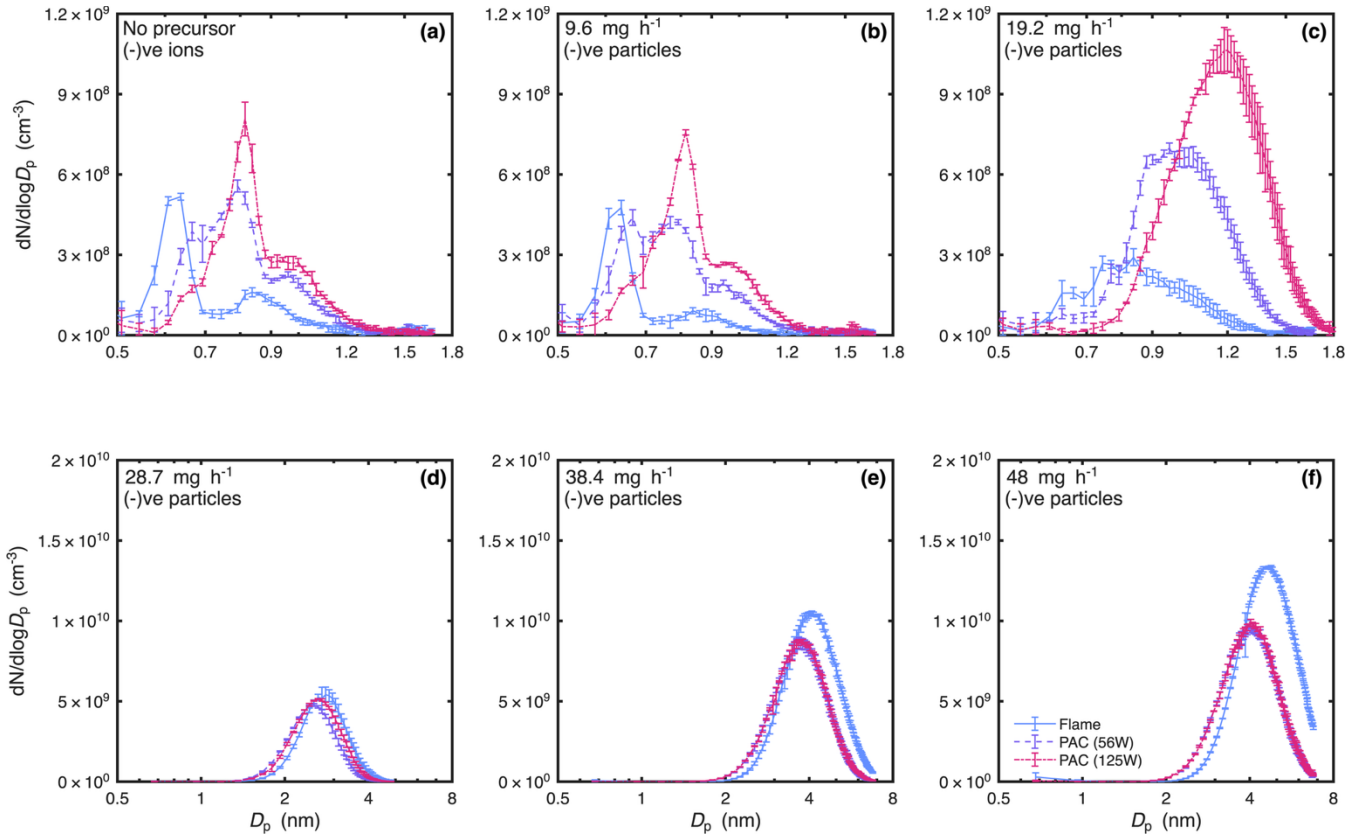

Figure 4: (a) The size distribution of negative ions without any TTIP; (b), (c), (d), (e), and (f) are the size distribution of negatively charged Ti-containing clusters with TTIP feed rates ranging from of 9.6 mg h^{-1} to 48 mg h^{-1}. Each panel compares the influence of corona discharge at power 56W and 125W on the size distribution. Error bars denote the standard deviation.

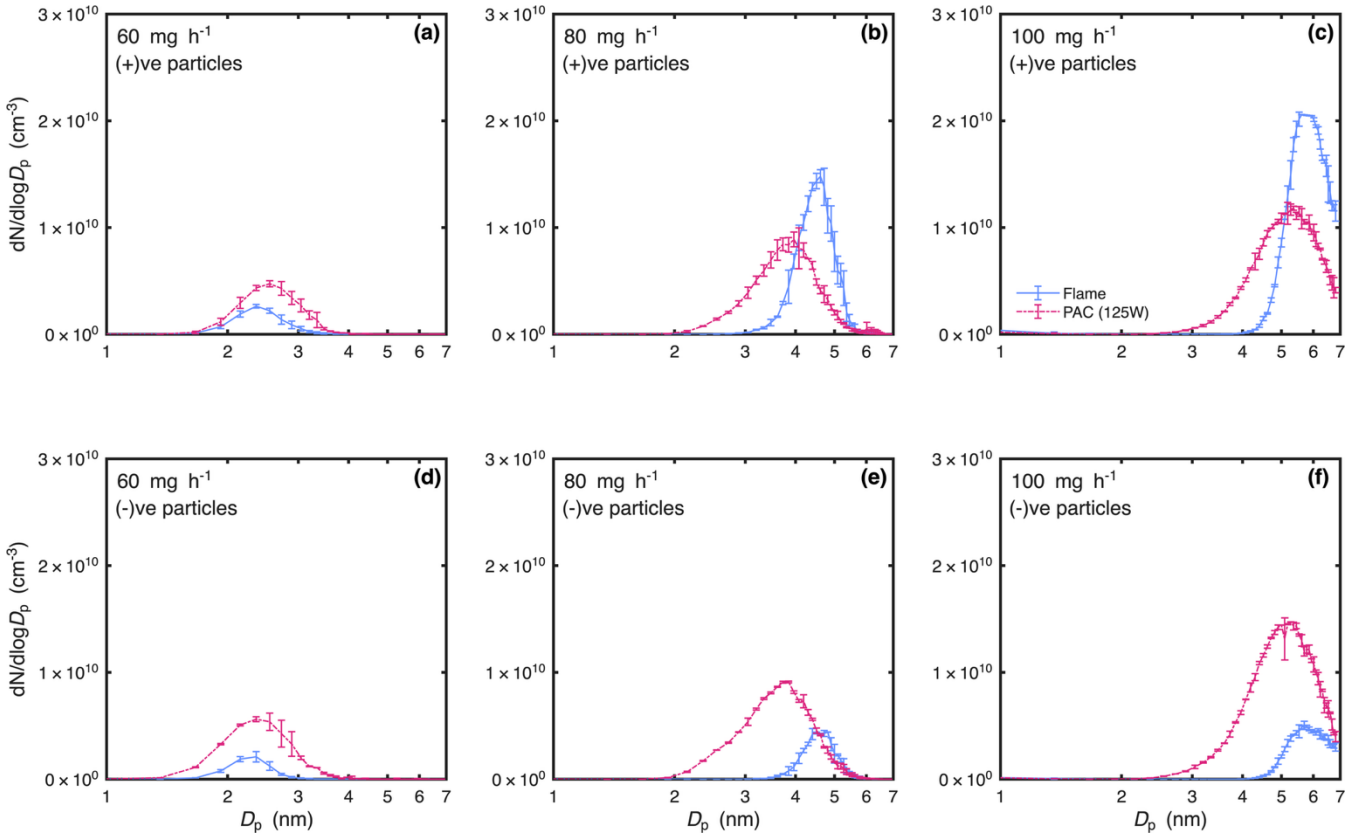

Figure 5: (a), (b), and (c) show the size distribution of positively charged Si-containing clusters; Similarly, (d), (e), (f) show the size distribution of negatively charged Si-containing clusters. The size distributions are shown for TEOS feed rates ranging from of 60 mg h^{-1} to 100 mg h^{-1}. Each panel compares the influence of corona discharge at power 56W and 125W on the size distribution. Error bars denote the standard deviation.

Comment 9: *With the same token, it would be nice to compare each SDF of the TTIP and TEOS nanoparticles (without correction for charged fraction) with that of the ions generated in the flame. How distinguishable is the raw signal of the nanoparticle from that of ions in the flames with the smallest nanoparticle precursor flow rates?*

Response: We have updated our Figs. 3 and 4 to show the size distribution of positive and negative ions along with size distribution of Ti-containing particles. Plots comparing the size distribution of ions along with size distribution of Si-containing particles are provided in the supplementary file (Figs. S4 and S5). Figs. 3 and 4 contain data that is corrected for charge fraction. Similar plots without correction for charged particles are included in the supplemental file (Figs. S2 and S3).

The updated figures are given below:

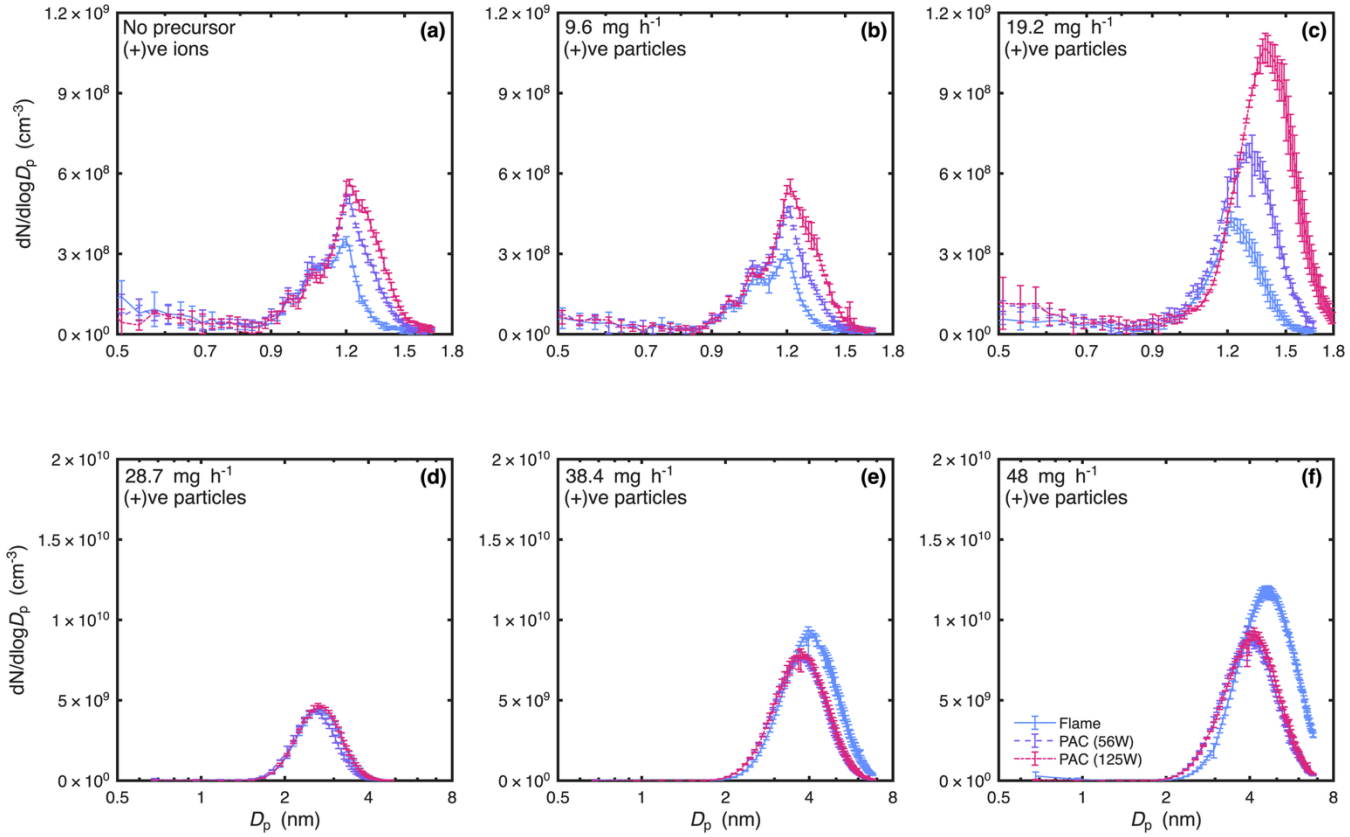

Figure 3: (a) The size distribution of positive ions without any TTIP; (b), (c), (d), (e), and (f) are the size distribution of positively charged Ti-containing clusters with TTIP feed rates ranging from of 9.6 mg h^{-1} to 48 mg h^{-1}. Each panel compares the influence of corona discharge at power 56W and 125W on the size distribution. Error bars denote the standard deviation.

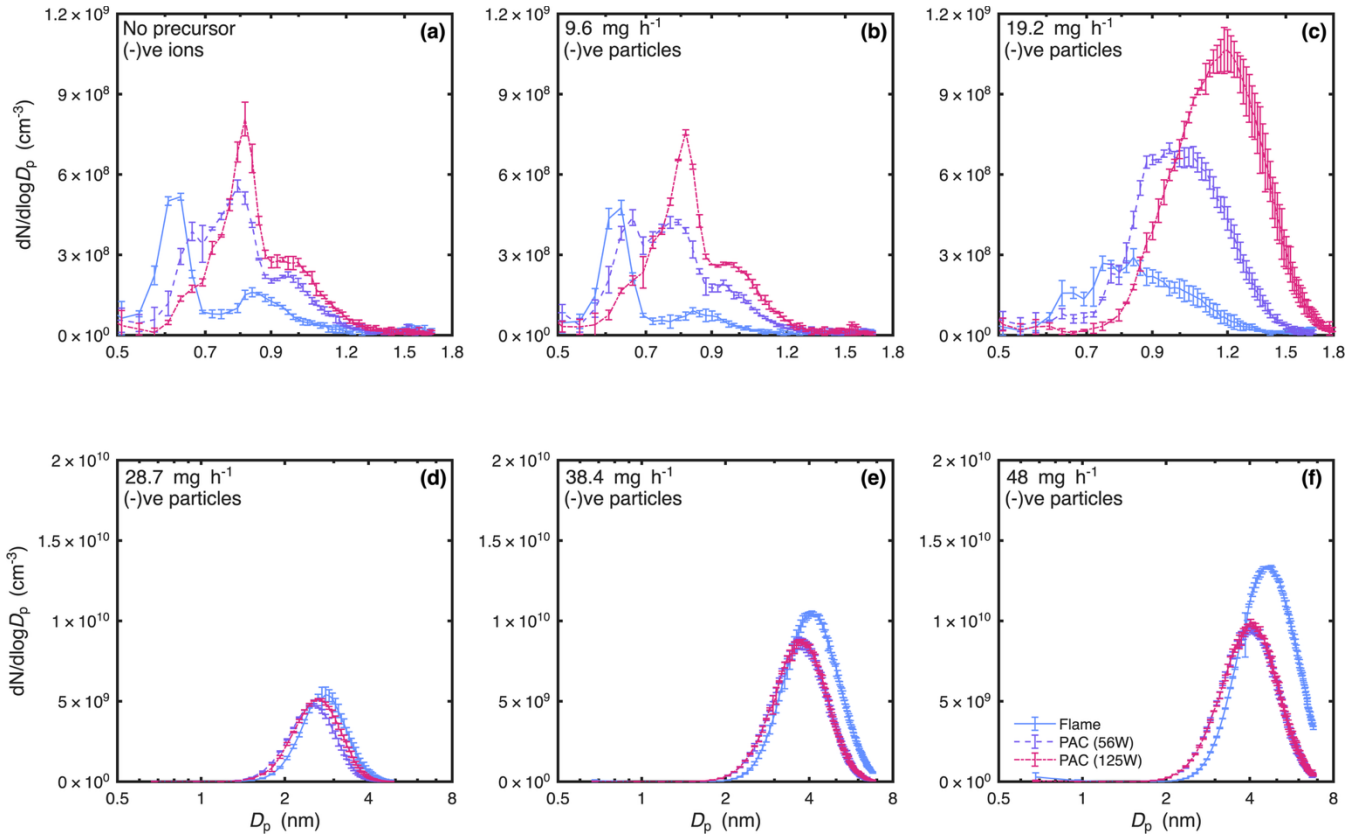

Figure 4: (a) The size distribution of negative ions without any TTIP; (b), (c), (d), (e), and (f) are the size distribution of negatively charged Ti-containing clusters with TTIP feed rates ranging from of 9.6 mg h^{-1} to 48 mg h^{-1}. Each panel compares the influence of corona discharge at power 56W and 125W on the size distribution. Error bars denote the standard deviation.

Comment 10: *Please describe Figure 5 more properly and include it in the manuscript where it is discussed first. What is the main message of this figure? How is the modal diameter determined? Can you include an error bar bracketing the standard deviation of the mobility diameter of the mode?*

Response: We thank the reviewer for pointing this out. Figure 5 (Fig. 6 in the current version of the manuscript.) has been moved closer to a location where it is first described.

The main message of the figure is how the modal diameter of an aerosol sample shifts based on the power of a corona discharge applied. The line plot is showing the percentage change in modal diameter with respect to the modal diameter obtained by particles produced from flame only condition. The modal diameter is the peak diameter from the size distributions in Figs. 3 and 4. As we obtain the peak modal diameter from an averaged data, we cannot include error bars to Fig. 6. We have added the following discussion to section 3.3 addressing these comments:

"Figure 6 shows the percentage change in modal mobility diameter, which is obtained from the number size distributions shown in Figs. 3 and 4. The modal diameter for each condition corresponds with the diameter which has the highest number concentration in the size distribution. From Fig. 6, we can see that when we introduced the high-frequency AC corona discharge in the flame, particle formation and growth were promoted under relatively lower precursor feed rates, $\leq$19.2 mg h^{-1}, but were suppressed under higher precursor feed rates, $\geq$ 28.7 mg h^{-1}, with respect to the particles generated from non-plasma combustion."

Comment 11: *The same argument applies also to fig. 6, which is plotted with a log-scale ordinate spanning 9 orders of magnitude, making it impossible to visualize any effect. Would it be wiser to have separate panels for the different considered charging mechanisms?*

Response: We agree with the reviewer that it would be easier to show the difference in charging levels by splitting Fig. 7 (was Fig. 6 in previous version of the manuscript) into four panels. Out of the four split panels, panel (a) and (b) show the diffusion charging effects. Panel (c) and (d) show the field charging effects. Here is the updated Fig. 7:

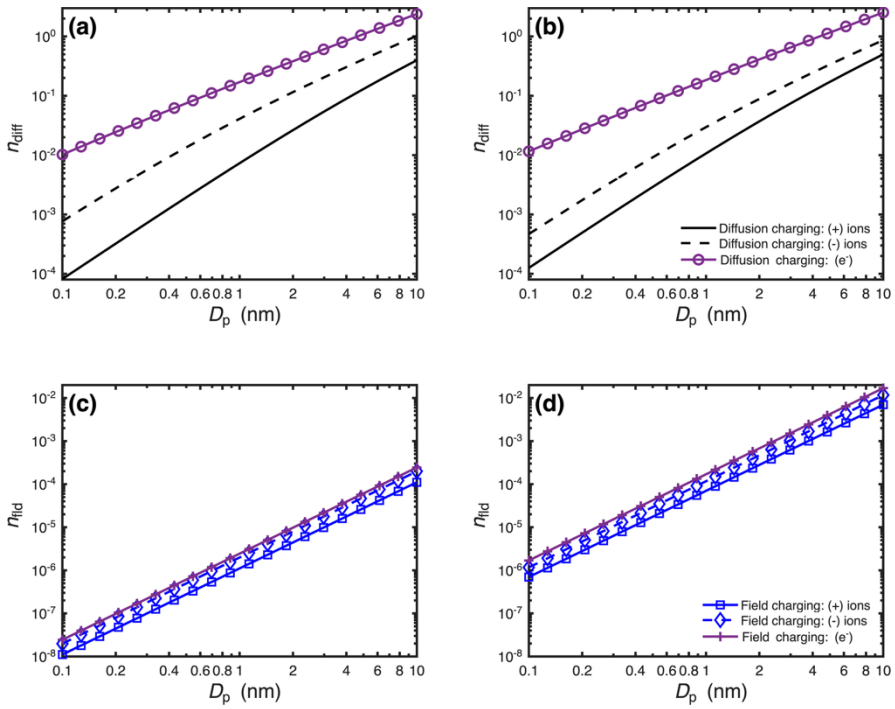

Figure 7: Shows the charge acquired by TiO_2 particles with a dielectric constant of 30; (a) Diffusion charging in flame only condition; (b) Diffusion charging in PAC with a plasma power of 125W; (c) Field charging in flame only condition; (d) Field charging in PAC with a plasma power of 125W.

Comment 12: *The manuscript discusses the expectation that the charging in negative polarity should be more efficient due to free electrons (e.g., in the last paragraph of page 13). Yet, if I did not get too lost in the wording, the experimental results do not support this expectation, especially those with TEOS in Fig. 4. Can you please clarify?*

Response: Yes, the charging in the negative polarity should be more efficient than in the positive polarity due to the free electrons. In a flame, electrons and negative ions together make up the total negative charge carriers in a flame. This leads to a greater number of positive ions being present in the flame than there are electrons. As a result, the negatively charged particles naturally tend to be lower in concentration than the positively charged particles. With few electrons being available to charge the metal oxide particles, a smaller number of particles will be charged and hence classified. Additionally, Si-containing particles are less conductive than Ti-containing particles. Compared to Ti-containing particles which have a dielectric constant value of 30 (assuming most of the Ti-containing particles are TiO_2), Si-containing particles tend to have a low dielectric constant value of 3.9 (assuming most of the Si-containing particles are SiO_2). The lower number concentration that we see for the negatively charged particles in Fig. 4 is likely due to the combination of the two above mentioned factors. The following description has been added to the manuscript's results and discussion section to clarify this question:

"We also see the concentration of negatively charged particles in flame only condition for the feed rates of 80 mg h^{-1} (Fig. 5b and 5e) and 100 mg h^{-1} (Fig. 5c and 5f) be much lower than that of positively charged particles. Despite electrons being excellent negative charge carriers, in a flame without plasma, the number of electrons is lower than that of the number of positive ions. This causes more Si-containing particles to be charged positive. Assuming that most of the Si-containing particles are SiO_2 and most of Ti-containing particles are TiO_2, the Si-containing particles have a very low dielectric constant of 3.9 compared to the Ti-containing particles which have a dielectric constant of 30. As a result, we see a huge concentration difference between the positively and negatively charged particles."

Comment 13: *Page 1, lines 10 and 18. Wording is not clear: "more stable" and "higher" compared to what?*
Response: We thank the reviewer for pointing this out. We have clarified the language at the mentioned lines.

"Adding plasmas to a flame has been shown to introduce high concentrations of charges, ions, and radicals to the said flame. This technique of adding plasma to a flame is called plasma-assisted combustion (PAC) and this addition has been shown to make a flame more stable and efficient."

"For the precursor feed rates used in this study (TTIP: 9.6 mg h^{-1} – 48 mg h^{-1}, TEOS: 60 mg h^{-1} – 100 mg h^{-1}), we found that particle growth is suppressed by the corona discharge under relatively higher precursor feed rates (above ~29 mg h^{-1} for TTIP and above ~80 mg h^{-1} for TEOS)."

Comment 14: *Page 2, line 34. I think the authors are referring to flame spray pyrolysis in turbulent conditions. Regardless, this statement should be supported by at least one citation. Also, the ensuing discussion may also benefit from distinguishing studies in laminar and turbulent (as well as premixed and non-premixed)*
Response: We thank the reviewer for pointing this out. We have added a reference to support our statement. The updated statement is as given below:

"Due to the rapid formation of aerosols within the coupled thermal and flow fields in combustion synthesis, the properties of the synthesized nanomaterials are sensitive to flame instability and fuel incomplete combustion, which may deteriorate the quality of the synthesized nanomaterials (Gröhn et al., 2014; Rittler et al., 2017; Serrano-Bayona et al., 2023)."

We agree with the reviewer that a discussion on laminar and turbulent flame will be helpful to the introduction section but in the interest of keeping the introduction short, we have decided to not include such discussion. We would like to keep our current introduction, where we discuss more about particle formation in combustion and plasma assisted combustion.

References:

Gröhn, A. J., Pratsinis, S. E., Sánchez-Ferrer, A., Mezzenga, R., and Wegner, K.: Scale-up of nanoparticle synthesis by flame spray pyrolysis: The high-temperature particle residence time, Ind. Eng. Chem. Res., 53, 10734–10742, https://doi.org/10.1021/ie501709s, 2014.

Rittler, A., Deng, L., Wlokas, I., and Kempf, A. M.: Large eddy simulations of nanoparticle synthesis from flame spray pyrolysis, Proceedings of the Combustion Institute, 36, 1077–1087, https://doi.org/10.1016/j.proci.2016.08.005, 2017.

Serrano-Bayona, R., Chu, C., Liu, P., and Roberts, W. L.: Flame Synthesis of Carbon and Metal-Oxide Nanoparticles: Flame Types, Effects of Combustion Parameters on Properties and Measurement Methods, https://doi.org/10.3390/ma16031192, 1 February 2023.

Comment 15: *Page 3, line 84. Do you mean 1E23 rather than 1023?*

Response: Thank you for identifying this error. We have fixed this.

"Depending on the type of plasma, the electron concentration can reach up to 10^{23} m^{-3}, with electron energies ranging from 0.8 eV to 10 eV."

Comment 16: *Page 3, line 93. Ion wind (and undiscussed space charge) effects may still be relevant under AC conditions. Regardless, this statement should be supported by at least one citation.*

Response: We thank the reviewer for pointing this out. We agree with the reviewer that ionic wind effects may still be present when using an AC power source, however they are negligible compared to conditions where a DC power supply is employed. The above statement was based on the study by Ohisa et al., (1999) and it is already cited on the same paragraph. However, we believe that the citation was not clear in the way that the paragraph was structured. We have rewritten the paragraph to clarify the citation and convey this message. The modified introduction section is as follows:

"Ohisa et al., (1999) show that these electrons and charged species are generated on the tip/edge of the electrodes, which are placed outside the high-temperature region, and how they are introduced into the flame depends on the type of power source used to generate the discharge. The same study shows that a difference in cation concentrations when using a DC power source is 10 times higher than it is when using an AC power source. This suggests that when a DC power source is used, the charged species are introduced to the flame via the ionic wind and in the case of an AC power source, the charged species enter the flame predominantly via diffusion (Ohisa et al., 1999). Though the ionic wind effects might still be present in case of an AC power source, they are not as dominant as the ionic wind effects in case of a DC power source. This difference in the concentration of charged species can lead to the plasma having different effects on particle formation and growth in combustion systems."

References:

Ohisa, H., Kimura, I., and Horisawa, H.: Control of Soot Emission of a Turbulent Diffusion Flame by DC or AC Corona Discharges, Combust. Flame, 116, 653–661, 1999.

Comment 17: *Page 9, line242. This is not surprising since electrons are more likely to affect the flame compared to much larger cations.*

Response: We thank the reviewer for pointing this out. We have removed this statement.

Comment 18: *Page 11, lines 280-282 and 293-24. To what suppression and promotion effects is the prose referring to?*

Response: The prose is referring to the promotion and suppressive effects that the corona discharge has on the particle formation and growth. We have rewritten this sentence for more clarity. Here's the updated description:

"We also examined the effect of the power of corona discharge on size distribution. We find that promotion and suppressive effects of particle formation and growth remain for plasmas of both powers, but the promotional effects are stronger for a corona discharge with the higher power of 125 W."

We thank the reviewer for these helpful comments. This has improved our manuscript and we look forward to the paper being accepted for publication.